Jurnal Tribologi 36 (2023) 43-56

MYTRIBOS Malaysian Tribology Society

Jurnal Tribologi

Website : jurnaltribologi.mytribos.org e-issn: 2289-7232

Experimental study of contact angle and surface energy of a single aramid fibre and its relation on frictional behaviour of fibre-fibre contact

Nurhidayah Ismail [1*], Matthijn B. de Rooij [2], Dik J. Schipper [2], Nurul Hilwa Mohd Zini [1]

[1] Fakulti Kejuruteraan Mekanikal, Universiti Teknikal Malaysia Melaka, Hang Tuah Jaya, 76100, Durian Tunggal, Melaka, MALAYSIA.
[2] Department of Mechanics of Solids, Surfaces and Systems (MS3), University of Twente, NETHERLANDS.
[*]Corresponding author: nurhidayah.ismail@utem.edu.my

KEYWORDS

Aramid fibre
Contact angle
Surface energy
Friction

ABSTRACT

Surface energy has a significant impact on the adhesion and friction behaviour of fibres in composite materials. Finding the surface energy of a single fibre, on the other hand, maybe challenging. In this work, the surface energy of single aramid fibre is calculated using dynamic contact angle measurements. The contact angles of three different types of Twaron® aramid fibres with varying treated materials and thicknesses are tested in a series of test liquids. As a result of the changing surface characteristics of the fibre, the surface energy of treated fibre is found to be approximately 37% greater than that of untreated fibre. The thickness of the fibre also affects its surface energy because thicker fibres have a larger contact area, which increases surface energy in the region of contact. At specific applied normal load conditions, it can be found that the coefficient of friction increased as the total surface energy in the area of the contact interface increased.

1.0 INTRODUCTION

Fundamentally, the adhesion force is the main force that holds the surfaces together, which could be used to define the required work to separate two surfaces from contacting each other. It is also one of the crucial factors in investigating the structural performance of fibrous materials. The adhesion behaviour depends on the solid surface (interface) properties, surface cleanliness,

Received 30 May 2022; received in revised form 24 August 2022; accepted 14 October 2022.
To cite this article: Ismail et al. (2023). Experimental study of contact angle and surface energy of a single aramid fibre and its relation on frictional behaviour of fibre-fibre contact. Jurnal Tribologi 36, pp.43-56.

total contact area, and also the environment. In addition, the surface energy, which is one of the surface properties, may also influence the adhesion behaviour of the fibre or any media that appears between them (Salimi, 2012). Note that at micro-and-nanoscale contacts, the adhesion force can be relatively high due to the significant surface area-to-volume ratio (Qiang et.al, 2012). For composites, the adhesion between the fibre surfaces could influence the functionality of adhesive bonding between fibres in a tow bundle, fibre to matrix, and fibre coating (Pieter et.al, 2007, Liu et.al, 2008, Caixia et.al, 2011). While aramid fibre (a type of fibrous material) often requires additional physical and chemical surface treatments to improve its wetting condition and ability to withstand high shear forces. This, however, will require a good understanding of the friction and adhesion forces between the fibres, which are also directly related to the surface energy.

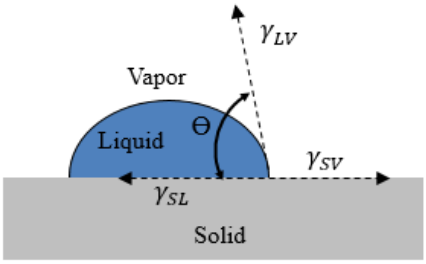

Figure 1: Contact angle of a solid surface - sessile drop method (Young, 1805).

The surface energy of a solid can be determined by measuring the contact angle between the solid and a series of test liquids e.g., distilled water and ethylene glycol, depending on the application purposes. To date, there are many established methods that can be used to measure the contact angle (Miller et.al, 1983, Hseih et.al 1991, van de Velde and Kiekens, 2000, Barraza et.al, 2001). However, the most extensively used by many is a sessile drop method, as it is a direct method to determine the contact angle. This method required a droplet of liquid to be presented on a solid surface as shown in Figure 1 (Young, 1805).

The liquid droplet adheres to the surface, and the contact angle may be calculated by measuring the angle between the tangent to the liquid-vapour (LV) interface and the solid-liquid (SL) interface. Because the contact angle is controlled by a static drop of liquid on the fibre surface, this is a static technique (Yuan and Lee, 2013). While the sessile drop method is appropriate for measuring the contact angle of a flat solid surface, it is challenging for measuring the contact angle of a cylindrical surface, such as a thin filament. Interestingly, experiments on modified aramid fibre surfaces using this technique (Hao et al., 2013) revealed that the volume of the liquid droplet affects both the drop shape and the macroscopic contact angle between the drop and the fibre. Furthermore, because the liquid is prone to evaporation, obtaining an accurate drop profile is challenging, and the result repeatability is limited. The Wilhelmy technique of finding the contact angle provides an option for this geometry (Wu, 1982). This approach determines the contact angle by measuring the wetting force imparted to the fibre during immersion and withdrawal from the liquid. This method has been used with carbon (Si et al., 2016 and Jian et al., 2017) and basalt (Monica et al., 2017) fibres, but not with aramid.

In this study, the surface energy of a single aramid fibre is determined utilizing the contact angle measurement. The role of surface energy in influencing the frictional behaviour of the aramid fibre is investigated.

2.0 EXPERIMENTAL DETAILS

Table 1 summarizes the material properties of the aramid fibre used. The contact angle of each fibre type was tested in three different test solutions: n-hexane, distilled water, and ethylene glycol. The properties of the test liquids are listed in Table 2. Each fibre type is tested three times with three different samples. All tested fibres are taken directly from the bobbin and cut into 10 mm lengths. Both X1 and X2 fibre originate from the same fibre and vary only in surface treated material.

Table 1: Characteristic of Aramid fibre used.

Description	Unit	X1	X2	X3
Young's modulus	GPa	109	109	29.3
Linear density	dtex	1.7	1.7	1.68
Breaking strength	N	0.39	0.39	15.4
Fibre diameter	um	12	12.2	140
Treated material		No	Alkyl-phosphate salt	ethoxylated/ propoxylated butanol

Table 2: Properties of the test liquids.

Test liquid	γ_L (mN/m)	γ_L^d(mN/m)	γ_L^p(mN/m)	ρ(g/cm^3)	η(mPas)
n-hexane	18.43	18.43	0	0.6603	0.3080
distilled water	72.80	29.10	43.70	0.9982	1.002
ethylene glycol	48.00	29.00	19.00	1.1088	21.80

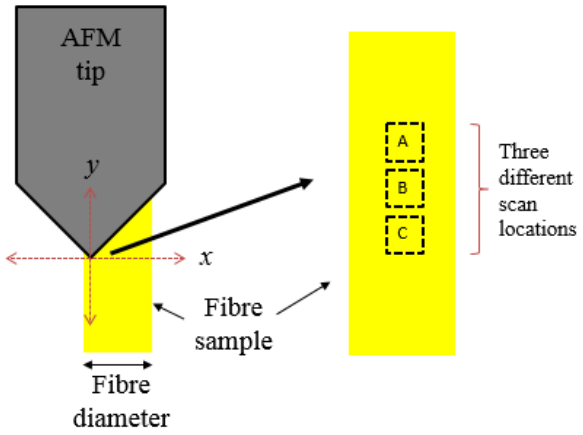

Figure 2: Schematic of AFM measurement.

Surface characteristics are measured using Nanosurf FlexAFM with ACTA cantilever type. The force constant of a cantilever is between 13 – 17 N/m with a width of 30 m and a length of 125 m is used. The areal roughness of the fibre is scanned along the x axis with a resolution of 512 x 512 points in a 3×3 scan size region, reducing the impact of fibre orientation on roughness assessment. The fibre is held vertically parallel to the AFM tip (see Figure 2), and roughness is evaluated at three separate points (A, B and C).

Figure 3 shows the schematic diagram of the dynamic wetting force experimental setup. The fibre is oriented perpendicular to the liquid interface and the force exerted on it during immersion and withdrawn due to wetting is measured by a tensiometer. In this experiment, the force measured is a combination of the wetting force, buoyancy force and a mass which can be expressed as Equation (1).

$$F = F\ capillary - F\ bouyancy + mass \quad (1)$$

Where γ_l is the surface tension of the test liquid, D is the diameter of the fibre and θ is the contact angle, m is the mass of the fibre, g is the gravitational acceleration, ρ is the density of the test liquid and $V_{immersed}$ is the immersed volume of the fibre. In this case, if 5 mm of fibre is immersed in distilled water, the buoyancy force found to be on the order of 10^{-9} N which is very small and can be neglected compared with the capillary force in the order of 10^{-5} N. Since the tensiometer is zeroed each time before starting the measurement, the mass contribution is zero. This means that the relationship between the force measured, F and the contact angle, θ can be shown as Equation (2).

$$F = \pi D \gamma_l cos\theta \quad (2)$$

The DCAT 11 by DataPhysics Instruments, GmbH, which has a resolution of 10^{-6} g and a lifting speed range of 0.7 um/s to 500 mm/min are used in this experiment. A speed of 0.05 mm/s was maintained during the immersion and withdrawal of the fibre. According to (Si et al., 2016), a dynamic contact angle less than 20 mm/min is regarded a static progressing contact angle. As seen in Figure 3(a), an adjustable height stage is used to position a vessel carrying the test liquid beneath the balance. As indicated in Figure 3(c), the fibre is adhered to the sample holder using adhesive glue and secured to the balance (d). Prior to beginning the measurement, the adjustable stage is raised a few millimeters above the bottom of the fibre. After immersion and withdrawal, the force is measured at constant speed. Each sample in a test liquid is measured five times. The immersion depth is adjusted to 5 mm, and a new liquid is used for each sample to avoid contamination effects. All measurements were conducted in a monitored and controlled environment maintained at a temperature of 22^{o} C in a vibration isolation chamber.

Relationship between contact angle, surface tension of the liquid and solid are best described in Equation 3.

$$\gamma_S = \gamma_L \cdot cos\theta + \gamma_{SL} \quad (3)$$

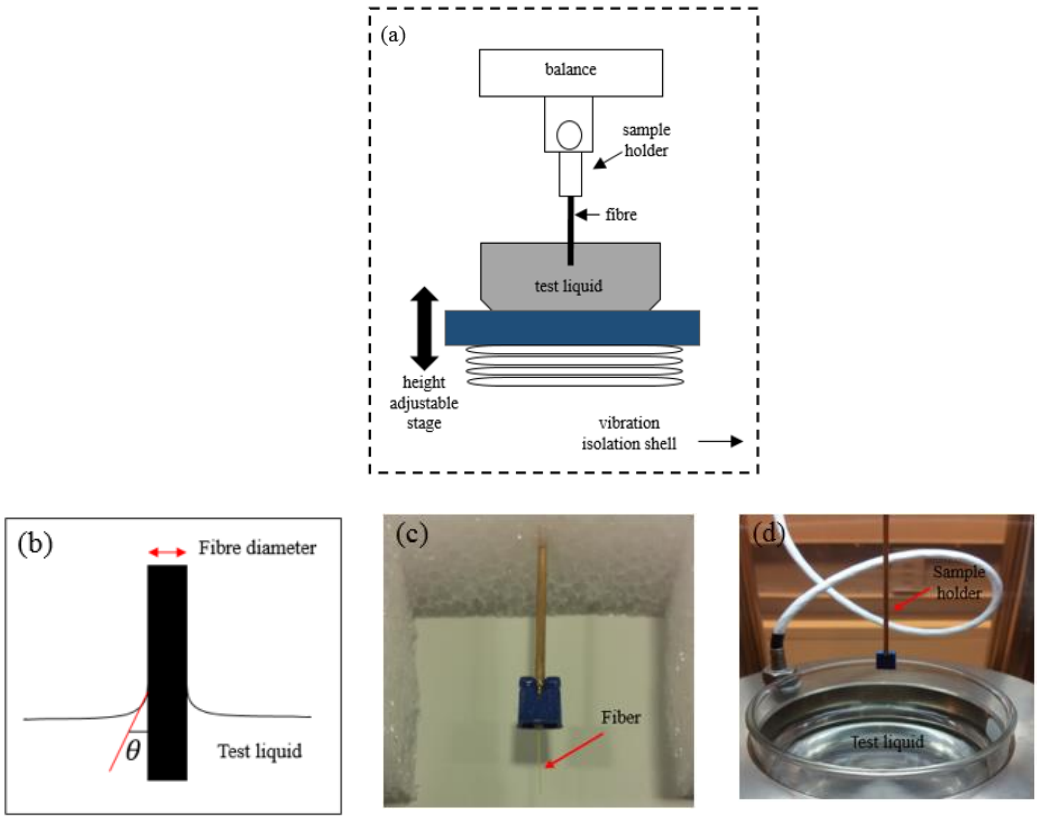

Figure 3: Schematic diagram (a) DCAT 11 setup, (b) contact angle, (c) and (d) image of aramid fibre glued on the sample holder.

Thus, in order to be able to calculate the surface free energy of a single aramid fibre, the unknown variable γ_{SL} must be determined. The interfacial tension is computed using the Fowkes method (Fowkes, 1964), based on the two surfaces tension γ_S and γ_L and the geometric mean of a dispersive part $\gamma^d$and a polar part γ^p of the surface tension as written in Eq. 4:

$$\gamma_{SL} = \gamma_S + \gamma_L - 2\left(\sqrt{\gamma_S^d \cdot \gamma_L^d} + \sqrt{\gamma_S^p \cdot \gamma_L^p}\right) \quad (4)$$

The combination of Equation 3 and Equation 4 leads to:

$$\gamma_L(1 + cos\theta)/2\sqrt{\gamma_L^d} = \sqrt{\gamma_s^p}\sqrt{\frac{\gamma_l^p}{\gamma_l^d}} + \sqrt{\gamma_s^d} \quad (5)$$

The contact angle value is calculated from the capillary force using Eq. 2 and inserted in the Owens-Wendt, so Eq. 5 (Owens and Wendt, 1969). At least two liquids with known dispersive and polar parts of the surface tension are required to determine the surface free energy of the solid, wherein at least one of the liquids must have a polar part larger than zero. According to (Chapman, 2014), using only two liquids result in an overestimation of the dispersive component and if more

liquids used, it increases the accuracy in the determination of fibre surface energy (Pasquini et.al, 2006).

3.0 RESULTS AND DISCUSSION

3.1 Roughness Measurement

Figure 4 (a) depicts a microscopic image of X1's surface structure generated by SEM. Figure 4 (b), (c), and (d) show the areal surface roughness measurements conducted by AFM on fibres X1, X2, and X3 at location B, respectively. The roughness measured has a root mean square (RMS) value of Sq 1.6 nm for X1, Sq 2.4 nm for X2, and Sq 3.7 nm for OC. When two identical fibre types, X1 and X2, are compared, it is clear that treating the fibre surface has no effect on surface roughness. The roughness is evident at the microscopic size, but on the order of nm. The results in Figure 4 (b), (c), and (d) show that there are lines and grooves on the surface of the fibre.

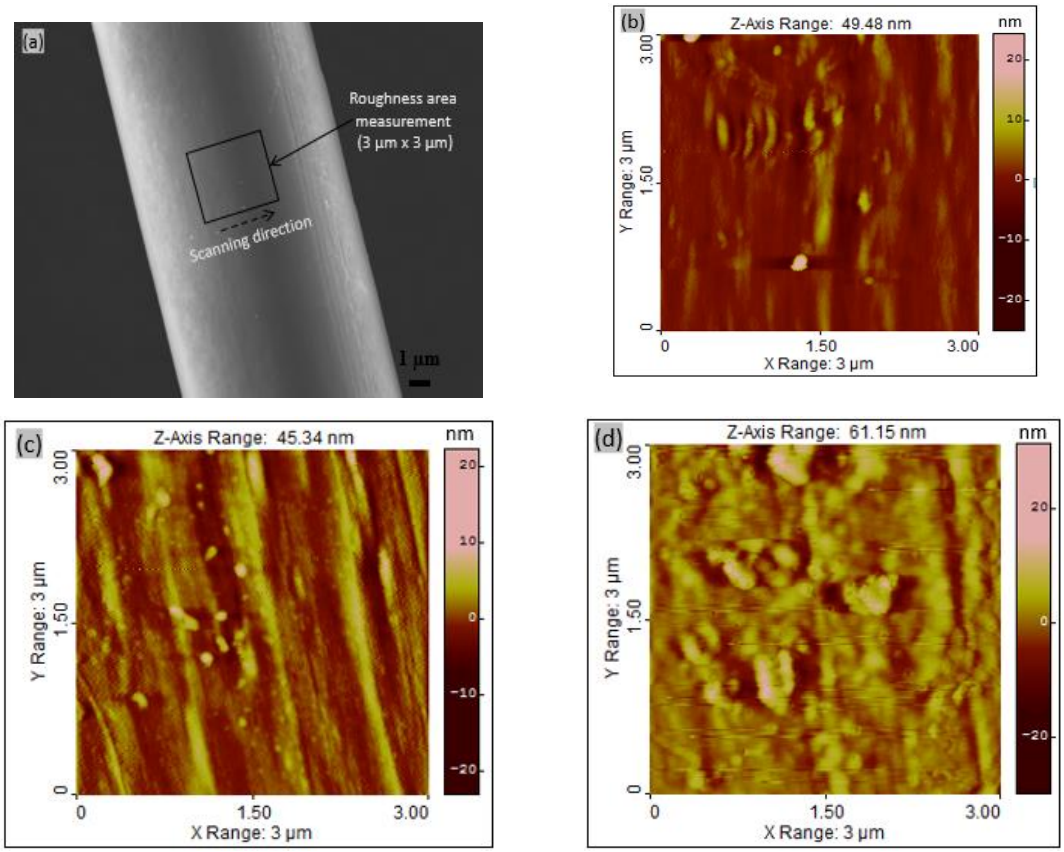

Figure 4: SEM and AFM images (a) SEM image of X2 fibre; Roughness measurements (b) X1, (c) X2 and (d) X3.

3.2 Contact Angle Measurements

The typical force measured as a function of the depth of immersion of an X3fibre type in water is shown in Figure 5. At first, the force signal is zero as the fibre approaches the test liquid. At 1.2 mm depth, the force signal significantly increases as the fibre makes contact with the test liquid surface and forms the contact angle. Following that, the force signal remains constant in value until the desired depth is reached. The procedure is then reversed, with the movable stage moving in the other direction and a continuous force signal representing the receding angle being monitored. When the fibre is removed from the liquid, as shown in Figure 5(b), the force signal continues to grow gradually. When the force signal reaches 0.8 mm, it abruptly drops to zero, seeming to be identical to the beginning of the test. This behaviour was caused by the fibre's snap off' from the test liquid. A modest increase in force just prior to the 'snap off' was attributable to the meniscus force generated during the separation of the fibre and the test liquid, as seen in Figure 5(b).

The data in Table 3 are for both advancing and receding contact angles. For untreated fibre X1, an average advancing contact angle of 65.1^{o} was recorded. This is somewhat higher than the previous researcher's measurement of 61.4^{o} using the sessile drop technique (Hao et.al, 2013). According to (van de Velde and Kiekens, 2000), capillary force rises linearly with filament diameter due to the increased wetted length. Interestingly, our results indicate that thicker fibres, such as X3 fibres, have a lower contact angle than X1 and X2 fibres. The decreased contact angle is considered to be attributed to the porosity of the X3 fibre, which is formed of microfilament or fine fibrils. Additionally, the advancing contact angle is somewhat greater than the receding contact angle; this difference is referred to as contact angle hysteresis (CAH). According to the literature, hysteresis is a thermodynamic irreversible process that occurs as a result of a variety of factors including surface roughness (Lam et al., 2001; Eral et al., 2013; and Xiadong et al., 2004), surface chemical heterogeneity (Neumann and Good, 1972), surface deformation, liquid adsorption and desorption, and molecular rearrangement (Lynn and Bernard, 1980 and Schwartz, 1980). It seems unlikely that the major cause of CAH in our study is due to surface roughness, given our AFM measurements indicate that the surface is microscopically smooth, with Sq values less than 5 nm for all fibres. Additionally, the molecular structure cannot be linked to the CAH, as aramid fibre is a highly crystalline aromatic polymer composed of immobile molecular chains (Lynn and Bernard, 1980). Thus, it is hypothesized that the CAH in this investigation originated from other sources, such as chemical heterogeneity on the surface.

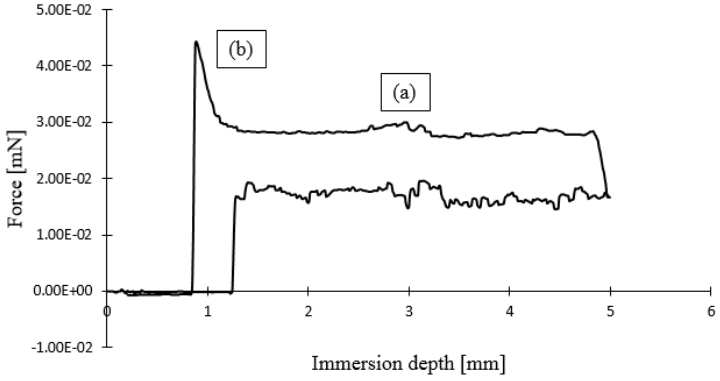

Figure 5: Force signal for X3 fibre type tested in water.

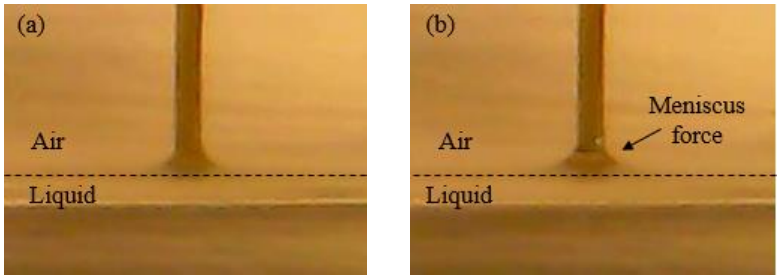

Figure 6: Real-time image of the meniscus formed between the X3 and water.

Table 3 Result of contact angle measurement

Fibre type	Contact angles (CA)± SD		
	CA advancing	CA receding	CA hysteresis
X1	65.1 ± 1.4	41.9 ± 4.7	23.2
X2	61.3 ± 1.5	31.4 ± 5.6	29.9
X3	35.8 ± 0.9	12.5 ± 1.1	23.3

*SD = Standard deviation

3.3 Surface Free Energy Analysis

Figure 7 shows plots obtained by applying contact angle values to calculate the surface energy of a single aramid fibre for three different test liquids using the Owens-Wendt technique. All of the results are consistent with the Owens-Wendt equation as defined in Eq. 5, with correlation coefficients more than 0.85 for all fibre types. As seen in Figure 7(b), an excellent match was attained for X1, a non-treated fibre type. The dispersive and polar components of the fibre surface energy estimated using the Owens-Wendt technique are shown in Table 4. Overall, the results indicate that the polar component has a greater value than the dispersive component. Additionally, it is discovered that the treated fibre X2 has a 12 mN/m greater total surface energy than the untreated fibre X1.

Table 4 The values of surface energy and its component (dispersive and polar).

Material	γ [mN/m]	γ^d [mN/m]	γ^p [mN/m]
X1	32.69	15.01	17.68
X2	44.69	12.83	31.95
X3	59.32	14.6	44.72

(a)
X1

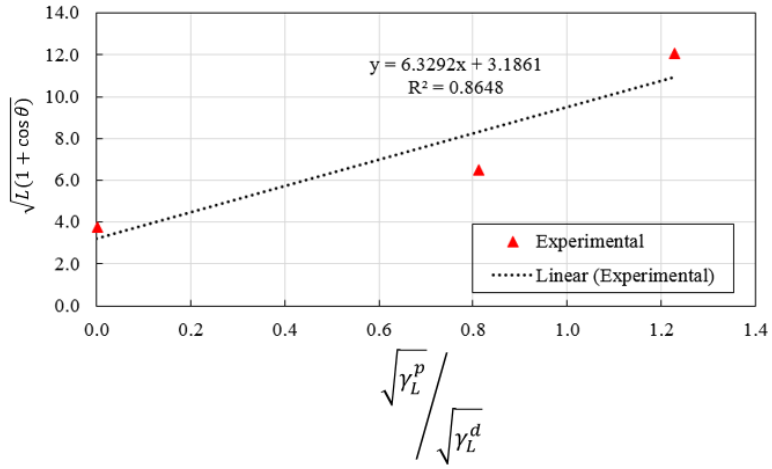

(b)
X2

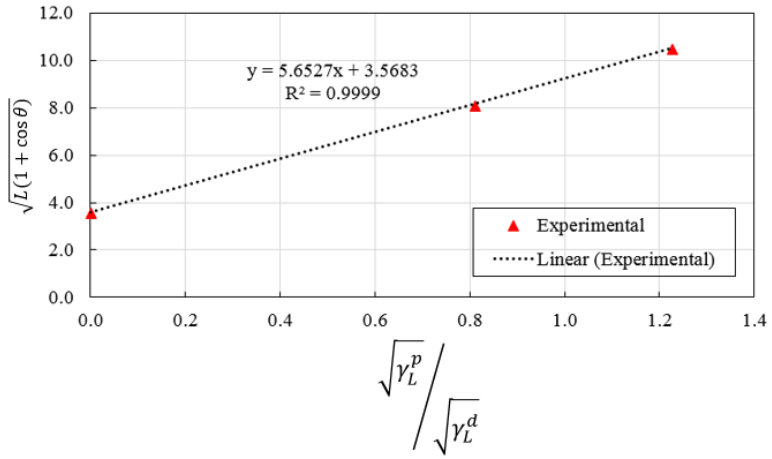

(c)
X3

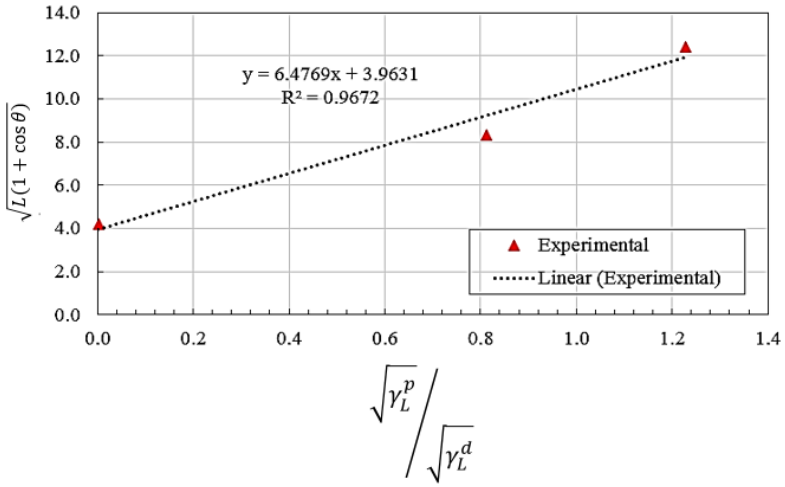

Figure 7: Linear fittings for surface energies of a single aramid fibre; (a) X1; (b) X2 and (c) X3.

3.4 Role of Surface Energy on Frictional Behaviour of Aramid Fibre

When the fibres' surfaces come into contact, a tangential force is necessary to begin motion between them. This force is composed of the normal force applied and the adhesion force. According to the most of adhesion models, including the Johnson-Kendall-Robert (JKR) model (Johnson and Kendall, 1971), the Derjaguin-Muller-Toporov (DMT) model (Derjaguin et al., 1975), and the Maugis-Dugdale (MD) model (Derjaguin et al., 1975), the adhesion force is proportional to the adhesion role (Maugis, 1992). One of the elements affecting this adhesion force is the surface energy. As a result, it is interesting to explore the function of surface energy in the frictional behaviour of two single aramid fibres, as revealed in this work.

The friction force between two single aramid fibres in sliding contact is determined using the designed experimental setup indicated in Figure 8 (Nurhidayah et al., 2019) under 10 and 15 mN loads. The experiment is conducted in ambient air at a temperature of 20°C with a sliding velocity of 2 um s^{-1} along a distance of 100 m. Table 5 shows the coefficients of friction for X1 and X2 fibre type. In this section the role of surface energy on frictional behaviour of X3 fibre type is not discussed due to the unavailable friction data of X3 fibre type. As can be seen, X1 fibre seems to have a lower coefficient of friction than X2 fibre.

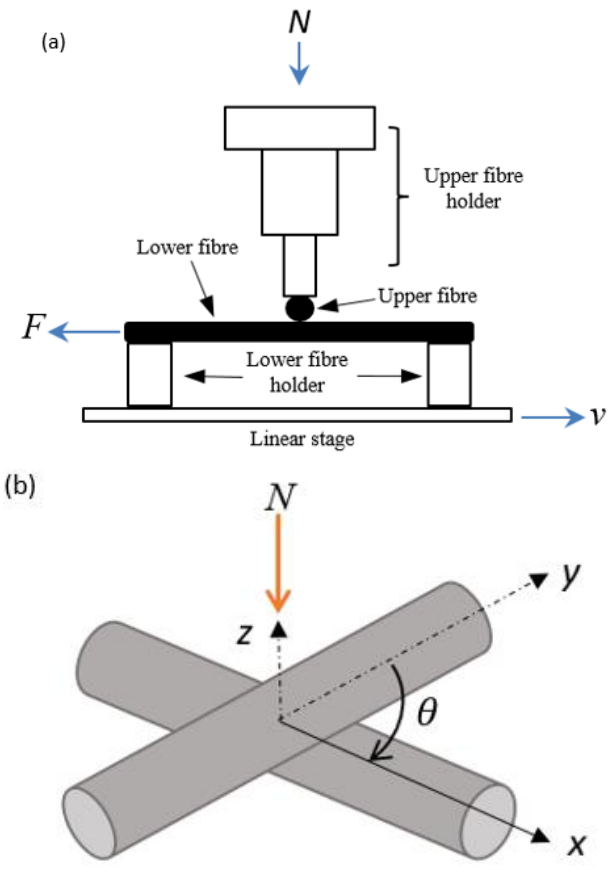

Figure 8: Friction between two single fibres (a) Experimental setup (b) fibre-fibre arrangement (Nurhidayah et.al, 2019).

Table 5 Experimental results.

Fibre type	**X1**	**X2**
Normal load [mN]	**Coefficient of friction, μ**	**Coefficient of friction, μ**
10	0.135	0.142
15	0.128	0.132

Given that friction force is proportional to contact area, i.e. $F = A$ (Bowden and Tabor, 1954, 1973); and that friction is solely caused by shear in the micro contact, where is the shear strength of the contact interfaces, a large contact area (at equivalent pressures) results in a higher friction force, i.e. a higher coefficient of friction. As was observed in (Miyoshi, 1999) for ceramic-metal couples in vacuum, the interfacial bond strength per unit area at the fibre-fibre interface could be directly related to the surface energy per unit area of a fibre. The contact area between two fibres sliding in perpendicular contact, A, can be simply calculated using the JKR circular contact model as follows (Johnson et al., 1971);

$$A = \left(\frac{3\pi R^*}{4E^*}\right)^{2/3} \left(N + 3\pi\Delta\gamma R + \sqrt{6\pi\Delta\gamma RN + (3\pi\Delta\gamma R)^2}\right)^{2/3} \quad (6)$$

with

$$\frac{1}{E^*} = \frac{1-v_1^2}{E_1} + \frac{1-v_2^2}{E_2} \quad (7)$$

and

$$R^* = \frac{R_1 R_2}{R_1 + R_2} \quad (8)$$

Where N is the normal load (N), $v_1 = v_2$ is the Poisson ratio of aramid fibre, $E_1 = E_2$ is the elastic modulus (GPa), $R_1 = R_2$ is the fibre radius (m) and $\Delta\gamma$ is the work of adhesion or the surface energy of the fibre.

Table 6 shows the calculated values for the area of contact between fibres obtained from JKR theory when a normal load of 10 mN or 15 mN is applied. Using this information, the role of the fibre's total surface energy inside the contact interfaces was analyzed. Total surface energy is defined as the product of the surface energy per unit area, γ and the contact area, A. The coefficient of friction, μ values obtained in Table 5 are used to calculate the total surface energy in the contact region, γA. The coefficient of friction for fibre-fibre interaction is plotted as a function of the total surface energy in the area of contact for a normal load of 10 mN and 15 mN, respectively. As the total surface energy in the area of the contact interface rose, the coefficient of friction increased as well. At a normal load of 10 mN, the coefficient of friction of the high surface energy fibre (X2) is 0.142, while the coefficient of friction of the low surface energy fibre (X1) is 0.135. It should be noted that the effect of the fibre's surface energy plays a role in raising the friction behaviour, as the X2 fibre's surface energy per unit area is 8.39 x 10^{-13} J, slightly greater than the X1 fibre's surface energy per unit area of 6.06×10^{-13} J. Without a doubt, when the surface energy is low, the interfacial bond strength per unit area is poor, as is adhesion and friction. Thus, the coefficient of friction is demonstrated to be approximately proportional to A, as demonstrated by (Miyoshi,

1999) in a vacuum investigation of ceramic-metal couples. This implies that the total surface energy between the fibre-fibre contact interface should be kept as low as possible to minimize friction.

Table 6 The calculated contact area between fibres obtained from JKR circular contact model.

Fibre type	**Area of contact, A_{JKR} (m^2)**			
Normal load applied, N [mN]	**1**	**5**	**10**	**15**
X1	4.073×10^{-12}	1.172×10^{-11}	1.854×10^{-11}	2.425×10^{-11}
X2	4.139×10^{-12}	1.188×10^{-11}	1.877×10^{-11}	2.455×10^{-11}

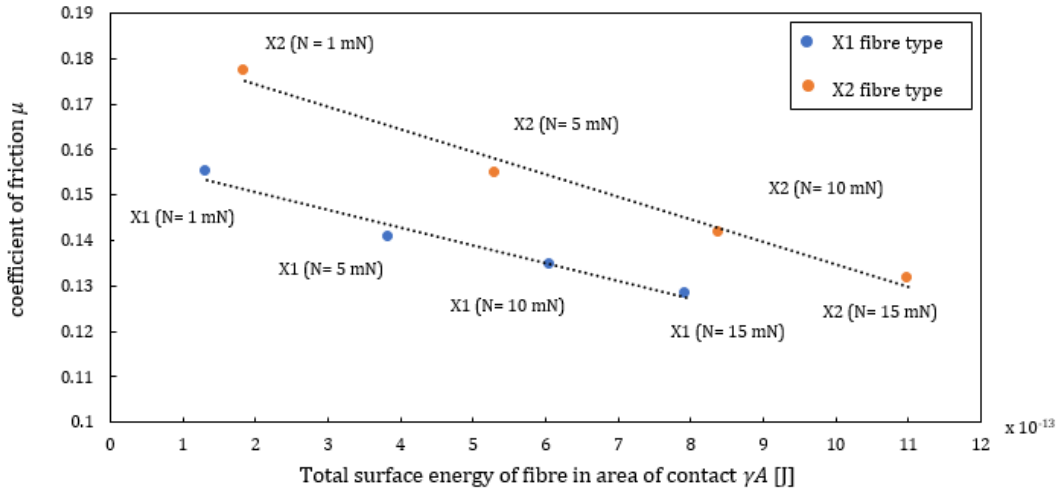

Figure 9: Coefficient of friction as a function of total surface energy of fibre in area of contact.

CONCLUSION

Due to the contact angle hysteresis phenomenon, the advancing contact angle is observed to be greater than the receding contact angle. In this study, hysteresis is assumed to be induced by surface chemical characteristics such as chemical heterogeneity, which influence contact angle variation when advancing and withdrawing. Twaron® aramid fibres have a predominantly polar surface energy and exhibit hydrophilic behaviour. The treated fibre surface has a higher surface energy than the untreated (virgin) fibre of the same type. It should be noted that surface energy also has an effect on the friction behaviour, with the coefficient of friction increasing as the total surface energy between the fibre-fibre area of the contact interface increases.

ACKNOWLEDGMENTS

The authors would like to express their enormous gratitude to Universiti Teknikal Malaysia Melaka and Ministry of Education Malaysia for financial support one of the authors, and also Teijin Aramid B.V for material supply.

REFERENCES

Barraza, H., J., Hwa, M., J., Blakley, K., O'Rear, E., A., Grady, B., P., (2001). Wetting behaviour of Elastomer modified glass fibre, Langmuir, 17(17),5288-5296.

Bowden, F., P., Tabor, D., (1954). Friction and lubrication of solids. Oxford, Clarendon Press.

Bowden, F., P., Tabor D., (1973). Friction: An introduction to tribology. Anchor Press. New York.

Caixia, J., Ping, C., Wei, L., Bin, L., Qian, W., (2011). Surface treatment of aramid fibre by air dielectric barrier discharge plasma at atmospheric pressure. Journal of Applied Surface Science, 257, 4165-4170.

Chapman II G., B., (2014) Non-destructive Evaluation of adhesive bonds using 20 MHz and 25 kHz ultrasonic frequencies on metal and polymer assemblies. ISBN 978-1-4969-2553-4.

de Gennes, P., G., (1985). Wetting: statics and dynamics. Rev. Mod. Physics. 57(3), 827-863.

Della, V., C., Maniglio D, Siboni, S., Morra, M., (2001). An experimental procedure to obtain the equilibrium contact angle from the Wilhelmy method. Oil & Gas Science and Technology – Rev. IFP, 56(1),9-22.

Derjaguin, B., V., Muller, V., M., Toporov, Y., P., (1975). Effect of contact deformations on the adhesion of particles. Journal Colloid Interface Science. 53, 314–325, 5.

Eral H., B., 'tMannetje, D., J., C., M., Oh, J., M., (2013). Contact angle hysteresis: A review of fundamentals and applications. Journal Colloid Polymer Science. 291(2), 243-260.

Fowkes, F., M., (1964). Contact angle, wettability and adhesion. Washington DC: American Chemical Society. p. 99.

Hao, W., Yao, X., Ke, Y., Ma, Y., Li, F., (2013). Experimental characterization of contact angle and surface energy on aramid fibres. Journal of Adhesion Science and Technology. 27(9), 1012-1022.

Hseih, Y-L., Wu, M., Andres, D., (1991). Wetting characteristics of Poly(p-phenyleneterephthalamide) single fibres and their adhesion to epoxy. Journal of Colloid Interface Science. 144(1),127-144.

Jian, W., Carlos, A., F., Dongxing, Z, Xungai W, Aart Willem VV, David S. (2017). Wettability of carbon fibres at micro- and mesoscales. Carbon. 120,438-446.

Johnson, K.L, Kendall K., Roberts, A., D., (1971). Surface energy and the contact of elastic solids. Proceedings of Royal Society London A. 324, 301–313 4.

Lam, C. N. C., Kim, N., Hui D, Kwok DY, Hair ML. (2001). The effect of liquid properties to contact angle hysteresis. Journal of Colloids Surface. A Physichochem Eng. Asp. 189: 265.

Liu, L., Huang, Y., D., Zhang, Z., Q., Jiang, Z., X, Wu, L., N., (2008). Ultrasonic treatment of aramid fibre surface and its effect on the interface of aramid/epoxy composites. Journal of Applied Surface Science. 254,2594-2599.

Lynn, S., P., Bernard, M., (1980). A study of the primary cause of Contact Angle Hysteresis on Some Polymeric Solid. Journal of Colloid and Interface Science. 78(1), 238-241.

Maugis, D., (1992). Adhesion of spheres: The JKR-DMT transition using a Dugdale model. Journal of Colloid Interface Science. 150, 243–269.

Miller, B., Penn, L., S., Hedvat, S., (1983). Wetting force measurements on single fibres. Colloidal. Surfaces. 6(1),49-61.
Miyoshi, K., (1999). Considerations in vacuum tribology (adhesion, friction, wear, and solid lubrication in vacuum). Tribology International. 32, 605-616.
Monica, F., P., Maria, C., S, Pierre-Jacque,s L., Fabrizio, S., Jacopo, T., Sylvain, D., (2017). Surface characterization and wetting properties of single basalt fibres. Journal of Composite Part B. 109:72-81.
Neumann, A., W., Good, R., J., (1972). Thermodynamics of Contact Angles I. Heterogeneous Solid Surface. Journal of Colloid Interface Science. 38(2),341-358.
Nurhidayah, I., Matthijn B., R., Erik, V., Nurul, H., M., Z., Dik, J., S., (2019). Friction between single aramid fibres under pre-tension load. Tribology International. 137, 236-245
Owens, D., K., Wendt, R., C., (1969). Estimation of the free surface energy of polymers. Journal of Applied Polymer Science. 13, 1741-1747.
Pasquini, D., Belgacem, M., N., Gandini, A., da Silva Curvelo, A. A., (2006). Surface esterification of cellulose fibres: characterization by drift and contact angles measurement. Journal of Colloid Interface Science. 295(1), 79-83.
Pieter, J. L., Peter, G. A., Edith, M., Shang-Lin, G., Warawan, P., Robert, J., Y. (2007). Controlled interfacial adhesion of Twaron aramid fibres in composites by the finish formulation. Journal Composite Science and Technology. 67, 2027-2035.
Qiang, S., Shing-Chung, W., Wei, Y., Jianwen, H., Jie, Z., Jinghua, Y., (2012). Mechanism of Adhesion between Polymer Fibres at Nanoscale Contacts. Langmuir. 28, 4663−4671.
Salimi, A. (2012). Characterization of nano scale adhesion at solid surface of oxidized PP wax/PP blends. International Journal of Adhesion and Adhesives. 33, 61−66.
Schwartz, A., M, (1980). Contact Angle Hysteresis: A Molecular Interpretation. Journal of Colloid Interface Science. 75(2),404-408.
Si, Q., Carlos, A. F., Dongxing, Z., Aart Willem, V. V., David, S., (2016). Wettability of a single carbon fibre. Langmuir. 32, 9697-9705.
van de Velde, K., Kiekens, P., (2000). Wettability and surface analysis of glass fibres, Indian Journal of Fibre & Textile Reseatch. 25(1), 8-13.
Wu, S., (1982). In: Polymer interface and adhesion. New York: Marcel Dekker. p.264.
Xiadong, W., Xiaofenand, N., Buxuan W. (2004). Contact angle hysteresis and hysteresis tension on rough solid surface, Chinese Journal of Chemical Engineering. 12 (5), 615.
Young, T., (1805). III An essay on cohesion of fluids. Philosophical Transactions of the Royal Society of London. 5, 65.
Yuan, Y., Lee, T. R., (2013). Contact angle and wetting properties. Surface Science. 51,3-34.